Applied Geochemistry 146 (2022) 105463

Contents lists available at ScienceDirect

Applied Geochemistry

journal homepage: www.elsevier.com/locate/apgeochem

Mercury, organic matter, iron, and sulfur co-cycling in a ferruginous meromictic lake

Delphine Tisserand [a], Stéphane Guédron [a,*], Eric Viollier [b], Didier Jézéquel [b,c], Sylvain Rigaud [d], Sylvain Campillo [a], Géraldine Sarret [a], Laurent Charlet [a], Daniel Cossa [a]

[a] ISTerre, Univ. Grenoble Alpes, Univ. Savoie Mont Blanc, CNRS, IRD, Univ. Gustave Eiffel, F-38000, Grenoble, France
[b] Université Paris Cité, Institut de Physique Du Globe de Paris, 1 Rue Jussieu, F-75238, Paris Cedex 05, France
[c] CARRTEL, INRAE et Univ. Savoie Mont Blanc, 75 Bis Avenue de Corzent, F-74200, Thonon-les-Bains, France
[d] Univ. Nîmes, EA 7352 CHROME, Rue Du Dr Georges Salan, F-30021, Nîmes, France

ARTICLE INFO

Editorial handling by Dr C S Eckley

Keywords:
Mercury
methylmercury
Redox
Iron
Sulfur
Organic matter
Lake pavin

ABSTRACT

Mercury (Hg) speciation in natural waters is controlled by redox conditions and microbiological activity. Water columns of meromictic lakes have large and stable redox chemical and biological gradients that allow the investigation of many Hg chemical transformations. In this study, Hg speciation (elemental Hg = Hg^0, methylated Hg = MeHg) and partitioning between truly dissolved (<3 kDa), colloidal (<0.45 μm and >3 kDa), and particulate (>0.45 μm) fractions, were determined throughout a high-resolution water column profile in the ferruginous meromictic Lake Pavin (Massif Central, France) in July 2018. Total Hg concentrations (THg) in water ranged between 0.4 and 8.8 pmol L^{-1}. The particulate phase represented 10–70% of the THg, with a peak found in the mesolimnion associated with the particulate organic carbon maximum. In the mesolimnion, the colloidal fraction represented 12–68% of THg, and the highest value was found at the top of the sulfidic zone, whereas the truly dissolved Hg species (70 ± 9%) dominated in all the rest of the sulfidic zone. MeHg ranged from less than 10% of THg in the oxic mixolimnion to more than 90% in the anoxic monimolimnion. The Hg methylation was most active within the suboxic zone where iron and sulfate reduction are occurring. These results, associated with those of the partition of organic matter (OM), sulfur, and iron, in conjunction with thermodynamic calculations, allow us to present a conceptual scheme for the Hg cycle in the lake. Atmospheric Hg deposited onto surface waters of the lake is partially photo-reduced and returned to the air, another part is scavenged by biogenic particulate matter and conveyed at depth by settling organic material. Water stratification and redox changes create a sequence of reactions from oxic to ferruginous waters where Hg is successively (i) desorbed from particulate OM where mineralization occurs, (ii) adsorbed onto iron-oxy(hydr)oxides, (iii) desorbed where they dissolved, (iv) precipitate as HgS, (v) methylated, and (vi) reduced as Hg^0 in the deepest part of the lake. In brief, the (micro)biological uptake, OM, iron and sulfur recycling, through associated microbial consortia, control the Hg cycling in the Pavin waters.

1. Introduction

Mercury (Hg) is present in natural waters mainly in two oxidation states (0 and II). The zerovalent form is the dissolved gaseous elemental Hg (Hg^0), and the divalent forms (Hg^{II}) are often tightly bound to sulfur (S) and carbon (C) (Wang et al., 2022; Xia et al., 1999). Hg^{II} forms preferentially strong complexes with reduced inorganic sulfur and organic matter (OM) via sulfhydryl (-SH) groups (Dyrssen and Wedborg, 1991; Riccardi et al., 2013). It also forms covalent bonds with C (Barone et al., 1996), which leads to the natural occurrence of the highly toxic methylated Hg (MeHg) compounds, including its two forms; i.e., monomethylmercury (MMHg), and the volatile dimethylmercury (DMHg). On the other hand, Hg–S affinity explains the dominant association of Hg with natural OM enriched in reduced S functional groups (Loux, 1998). The biogeochemical cycle of Hg in natural waters involves numerous thermal, photo, and biogenic reactions. Among them, two reversible and competitive Hg transformations are crucial from an aquatic ecology point of view: oxidation-reduction and methylation-demethylation. Indeed, reduction of Hg^{II} leads to the

* Corresponding author.
E-mail address: stephane.guedron@ird.fr (S. Guédron).

https://doi.org/10.1016/j.apgeochem.2022.105463
Received 15 July 2022; Received in revised form 6 September 2022; Accepted 8 September 2022
Available online 13 September 2022

Terminology of mercury chemical species

THg	Total Hg (all Hg species)
MMHg	Monomethyl Hg
DMHg	Dimethyl Hg
MeHg	Methylated Hg (MeHg = MMHg + DMHg)
Hg^0	Elemental Hg
Hg^{II}	Divalent Hg
DGM	Dissolved Gaseous Hg (DGM = Hg^0 + DMHg)
THg_F	Total Hg in filtrated (0.45 μm)
THg_P	Total particulate Hg (>0.45 μm)
$MeHg_F$	Methylated Hg in filtrated (0.45 μm)
$MeHg_P$	Methylated particulate Hg (>0.45 μm)
THg_{UF}	Truly dissolved Hg, *i.e.,* ultrafiltered samples (<3 kDa)
THg_{coll}	Colloidal Hg, *i.e.,* fraction >3 kDa and <0.45 μm
$THg_{F\ Res}$	THg_F - $MeHg_F$
$THg_{P\ Res}$	THg_P – $MeHg_P$

formation of volatile Hg^0 that can escape from the aquatic environment, and methylation leads to the formation of MMHg that, through its biomagnification in aquatic food webs, is harmful to fish consumers. For this latter reaction, microbial activity is crucial and largely dominates abiotic production (Cooper et al., 2020; Parks et al., 2013; Regnell and Watras, 2018; Ullrich et al., 2001). These reactions occur particularly in hypoxic and anoxic environments (Fitzgerald et al., 2014; Mason et al., 2012), making the Hg cycling in natural waters strongly dependent on redox conditions (Mason et al., 1999). In addition to reactions occurring in the dissolved phase, Hg may precipitate as sulfur minerals (*e.g.*, cinnabar) in euxinic environment, and is involved in heterogeneous reactions, such as sorption onto various minerals, including iron minerals like goethite (Kim et al., 2004; Slowey and Brown, 2007) and mackinawite (Jeong et al., 2007). Numerous studies have documented the main Hg changes in speciation and partitioning where strong redox gradients are present, such as in surficial sediments of lakes and coastal zones (Feyte et al., 2010; Gobeil and Cossa, 1993; Merritt and Amirbahman, 2007). However, the complexity and diversity of Hg transformations are difficult to distinguish in sedimentary deposits where redox changes occur at millimeter or centimeter-scale. On the contrary, they are easily characterized at high resolution in water columns where redox gradients may extend over several meters. Indeed, Hg enrichment and major changes in speciation have been identified at the interfaces between oxic and anoxic waters (Cossa and Coquery, 2005; Guédron et al., 2020b; Iverfeldt, 1988; Lamborg et al., 2008; Mercone et al., 1999; Muresan et al., 2008). The high-resolution (1 cm) study of a stratified water column in a tropical dam lake, showed prominent Hg methylation intricately linked with Hg^0 production at the chemocline (Muresan et al., 2018). Both reactions were found to be fueled by nutrients released episodically during the decomposition of settling OM or inhibited by dissolved OM and inorganic compounds continuously transported from the deeper layer. Hence, the chemocline acts as both an accumulation and recycling domain for settling MeHg-loaded organic particles.

The water column of meromictic lakes is permanently stratified. Lake Pavin (France) is a good example of such a situation; it offers a unique natural geochemically well-described laboratory (Bura-Nakic et al., 2009; Busigny et al., 2016; Jézéquel et al., 2016; Viollier et al., 1997), where Hg transformations can be studied in detail. Only one study has previously described the distribution of the Hg species in Lake Pavin (Cossa et al., 1994). With the analytical tools available at that time, the authors described the MeHg formation at the redoxcline and suggested an influence of Fe and Mn recycling on Hg partitioning and speciation. More recently, HgS nanoparticles have been identified in the monimolimnion (Miot et al., 2016). The present study is the first to focus on Hg distribution, speciation, and partitioning in the oxic-anoxic transition zone of a meromictic lake using 1 m vertical resolution profiles and which documents their relation to Fe, S, and OM redox cycling. In addition, the use of thermodynamic calculations codes on this dataset allowed us to better understand dissolved speciation and solution equilibrium state with respect to mineral phases in order to construct a comprehensive biogeochemical model for Hg cycling in the lake.

2. Material and methods

2.1. Study site

Lake Pavin (45°55′N, 2°54′E, Fig. 1) is a trachytic maar, located in the Massif Central (France), at an altitude of 1197 m. The lake was formed ~6900 years ago (Chapron et al., 2010; Juvigné et al., 1996) during a strong phreatomagmatic explosion (Thouret et al., 2016). The lake is a nearly circular depression of *ca.* 750 m in diameter and 92 m depth, with an area of 0.445 km^2 and a truncated cone topography. Its watershed is estimated to be 1.24 km^2 (Michard et al., 1994). The average discharge of Lake Pavin is 50 L s^{-1} (Thouret et al., 2016). Because of its geometry, wind protection, and sub-lacustrine springs, the mixing of the Pavin water column is depth-limited (Bonhomme et al., 2016; Busigny et al., 2016). Lake Pavin is a ferruginous meromictic lake, composed of two main layers: (i) the mixolimnion, which extends from the surface to 50–60 m depth and is oxygenated due to the seasonal mixing, and (ii) the permanently anoxic monimolimnion, which extends down to the lake bottom (92 m) and contains very high concentrations of dissolved elements which contribute to the stability of the layer (Martin, 1985; Michard et al., 1994; Viollier et al., 1997). The residence time of the waters is estimated between about 9 years in the mixolimnion and 100 years in the monimolimnion (Jézéquel et al., 2016). In between, is a transition zone, called the mesolimnion (sometimes considered as the upper part of the monimolimnion), which is characterized by a strong decrease in oxygen and redox potential, and a strong increase in specific conductivity (Busigny et al., 2022; Lopes et al., 2011). It is worth noting that the vertical positions of the oxycline, the redoxcline and the chemocline in the water column may change by a few meters depending on seasons (Bonhomme et al., 2011).

2.2. Sample collection and storage

Sampling was performed in July 2018 from the middle of the lake (Fig. 1) on a floating platform using a PFA pneumatic pump (AstiPure™, Saint-Gobain) with a 100-m-long polyethylene (0.9 cm diameter) tubing. Samples were collected without any contact with the atmosphere at 1 m depth-intervals in the mesolimnion (52–65 m), and 10 m depth intervals elsewhere. Redox potential (Eh), conductivity, and pH were measured *in situ* with probes connected to a WTW multi 340i. Filtrations for Hg speciation, anions, major, trace, and redox-sensitive elements were performed on site onto hydrophilic 0.45 μm PTFE filters (Omnipore™). Filters were then used for the analysis of total particulate Hg (THg_P), and particulate major and trace elements. Filtered and unfiltered samples for total Hg (THg_F and THg_{UNF}) and methylmercury ($MeHg_F$ and $MeHg_{UNF}$) analyses were collected and stored into acid-cleaned FEP Teflon bottles following ultra-clean techniques (Cossa and Gobeil, 2000). In the mesolimnion, additional samples were ultra-filtrated on site on pre-cleaned membranes (<3 kDa, Vivaspin®, polyethersulfone (PES), by centrifugation (6900 rpm, 4 °C during 60 min), for the determination of the "truly-dissolved" THg (THg_{UF}) (Guédron et al., 2016). The colloidal part of the THgF, i.e., THg_{coll}, was then obtained from the difference between THg_F and THg_{UF}. All samples for Hg analysis were acidified (0.4% v/v) on-site with HCl (Optima® grade), except those for dissolved gaseous mercury (DGM = Hg^0 + DMHg) determinations, which were kept unfiltered in the dark at +4 °C until the analysis. Samples for major and trace elements were stored in polyethylene vials and acidified with HNO_3 (1% v/v, Suprapur® grade).

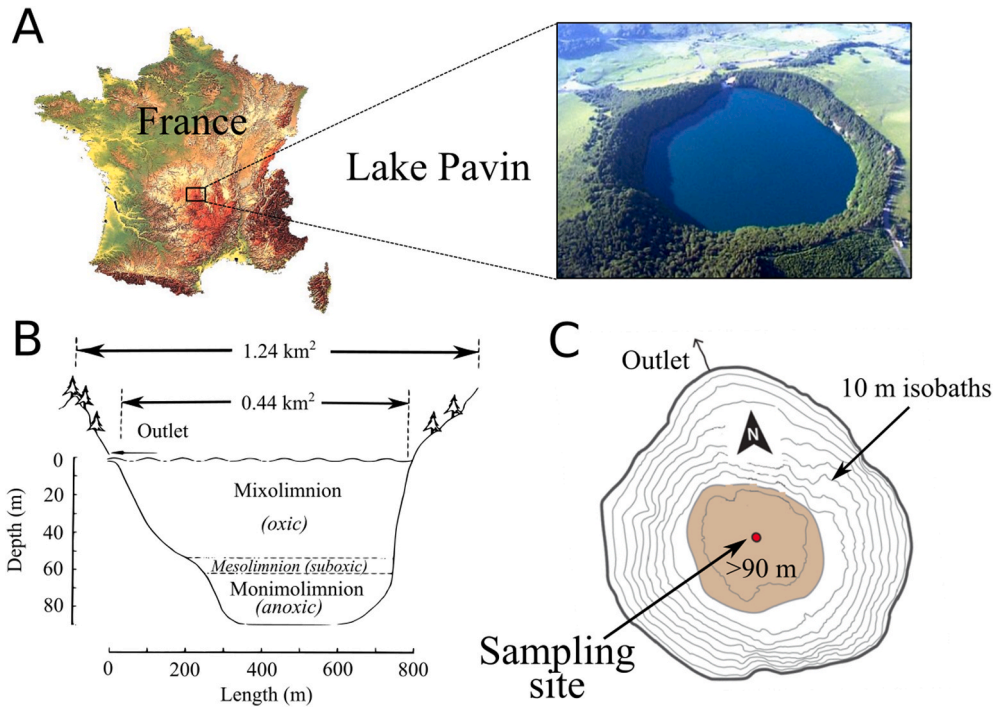

Fig. 1. Lake Pavin: A) location in the Massif Central (France) and aerial photography (Credit: D. Jezequel, CNRS Images), B) morphological characteristics of the lake, and C) bathymetric map and sampling site location adapted from Chassiot et al. (2016).

Samples for dissolved organic carbon (DOC) analyses were filtered through glass fiber filters (<0.7 μm, GFF). Filters were then cut in equal parts used for the analysis of particulate organic carbon (POC), THg_P and particulate methylmercury ($MeHg_P$). DOC samples were stored in borosilicate vials and acidified with HCl (0.2% v/v). All samples were wrapped in double bags and kept in the dark at +4 °C until analysis.

2.3. Mercury speciation and partitioning

Filtered, unfiltered, and ultra-filtered THg, and DGM in water were measured by CV-AFS (Tekran®, model 2500) following the published US-EPA Standard Method N° 1631 (Bloom, 1996; Cossa et al., 2003; USEPA and USEPA, 2002). The detection limit was 0.5 pmol L^{-1} for a 40-mL water aliquot and the reproducibility varied between 5 and 15% (N = 6) according to the concentration level in the samples. The accuracy of THg measurements was tested using the certified reference material (CRM) ORMS-5 (certified value = 26.2 ± 1.3 pg g^{-1}) from the National Research Council of Canada. DGM was quantified by purging 500 mL of unfiltered water with Hg-free argon within 2 h after sample collection (Cossa et al., 2017). Filtered and unfiltered MeHg (= MMHg + DMHg) were quantified following the derivatization method based on an aqueous ethylation, and purge-trap on a Tenax®, gas chromatography, and cold vapor atomic fluorescence spectrometry (CV-GC-AFS) with a Tekran® detector (model 2700) following the US-EPA 1630 protocol (USEPA and USEPA, 1998). The precision of analysis was determined by measuring replicates of a control standard (RSD <10%, N = 20), and the absence of matrix effect was verified using the standard addition technique (Guédron et al., 2011, 2017). Total particulate Hg and MeHg (THg_P, $MeHg_P$) concentrations were determined with the same method as for solution, after the digestion of Hydrophilic PTFE membranes with HNO_3:HCl mixture (2:1 v:v, 70 °C, 48 h) for THg_P, and after the digestion of GF/F membranes with HNO_3 (6 N, 70 °C, 24 h) for $MeHg_P$. The QA/QC was checked with two CRMs, MESS-3 and IAEA-405, for THg and MeHg respectively. Recovery was 100 ± 10% for the two methods, and precision was better than 15% for THg_P (n = 6) and better than 5% for $MeHg_P$ (n = 5).

2.4. Major, trace elements, and organic matter analyses

Particulate major and trace elements were quantified on an aliquot of the digestion solution used for the THg_P determination (PTFE filters). Total Fe and Mn concentrations and trace elements (Cu, Cd, Co, Ni, Zn, Pb, Cr) were quantified with an ICP-MS (Thermo®, X-series 2). Precision was assessed by replicate analysis of CRM SLRS-4, with values better than 7% for all studied elements. Major (Ca, K, Mg, Na, P, S, Si, Sr) were quantified by inductively coupled plasma atomic emission spectrometry (ICP-AES, Varian 720 ES model). The precision was better than ±5%. Ferrous iron (Fe^{II}) was determined on-site using the ferrozine method (Viollier et al., 2000) with a portable spectrophotometer. Sulfides ($\Sigma H_2S = H_2S + HS^- + S^{2-}$) samples were measured on-site with a portable spectrophotometer following Cline's method (Cline, 1969) on filtered water stabilized directly after filtration with 0.01 M zinc acetate (Tisserand et al., 2021). Calibration was performed using an external standardization from a solution prepared with $Na_2S.9H_2O$ and titrated by an iodometric method (USGS, 2002). Anions [(i.e., chloride (Cl^-), sulfates (SO_4^{2-}), nitrates (NO_3^-), and total dissolved phosphates (TDP)] were measured by ion chromatography (IC 332, Metrohm®), with a precision better than 1%. DOC was measured with a TOC-VCSN analyzer (Shimadzu®). POC and was quantified with a mass spectrometer (SERCON®) after combustion of GF/F filters at 1000 °C (Raimbault et al., 1999). The detection limit and precision were estimated at 10 μg and 5%, respectively. Finally, suspended particulate matter (SPM) was reconstructed from the organic and inorganic content of particles collected on filters (Prahl et al., 1997).

2.5. Thermodynamic calculations

Wham 7 (Tipping, 1994) and PhreeqC 3.0 (Parkhurst and Appelo, 2013) softwares were combined following the method of crossed modeling described in Rigaud et al. (2013) for the determination of (i) aqueous Hg^{II} and MeHg speciations, and (ii) mineral phase equilibrium accounting for redox gradient and dissolved OM complexation. The Thermoddem default database (https://thermoddem.brgm.fr/) was used and implemented with all reactions involving dissolved Hg and MeHg

known in the literature Tab. SI1 and 2 (Blanc et al., 2018; Drott et al., 2013; Feyte et al., 2012; Skyllberg, 2008; Smith and Martell, 1976)]. Calculations were firstly performed with WHAM and the calculated apparent thermodynamic constants (K_{app}) of the complexation reactions between aqueous Hg^{II} and MeHg and humic acid (HA) and fulvic acids (FA) were then added to the database for PHREEQC calculations. Temperature, pH, dissolved molar concentrations in dissolved inorganic Hg (THg-MeHg) and MeHg, HA, FA, Hg, Fe, Mn, ΣH_2S, major cations and anions were defined as input parameters in both models (Tabs. SI.3 and 4). HA and FA molar concentrations were calculated from Eqs. (1) and (2):

$$HA^{-1}_{mol\ L} = 2 \times 0.1 \times DOC^{-1}_{mg\ L} \times 10^{-3}/M^{-1}_{HA\text{-}g\ mol} \quad \text{(Eq. 1)}$$

$$FA^{-1}_{mol\ L} = 2 \times 0.9 \times DOC^{-1}_{mg\ L} \times 10^{-3}/M^{-1}_{FA\text{-}g\ mol} \quad \text{(Eq. 2)}$$

Considering a dissolved organic matter to DOC ratio of 2:1, and a FA:HA mass ratio of 9:1 with M_{HA} = 650 g mol^{-1} and M_{FA} = 2000 g.mol^{-1} (Buffle and Chalmers, 1988; Malcolm, 1985). Saturation indices (SI) were calculated for 47 mineral phases containing Hg, Fe, S, and Mn, including 11 H g mineral phases (Tab. SI2).

3. Results

3.1. Water column chemistry

Fig. 2 illustrates the successions of the redox (Fig. 2A) and physical (Fig. 2B) structures of the water column of Lake Pavin during the sampling period. The mixolimnion was spread between 0 and 53 m depth and the monimolimnion from 53 m down to 92 m including the mesolimnion between 54 m and 65 m. The aerobic limit was observed at 53 m (Fig. 2). The water conductivity was stable in the mixolimnion with an average value of 60 µS cm^{-1}, and increased in the mesolimnion to reach 470 µS cm^{-1} in the monimolimnion (Fig. 2C). Major elements concentration profiles in the filtered fraction depicted similar patterns parallel to the conductivity (Fig. SI1). The pH decreased from 7.0 at the surface to 6.1 at the bottom of the lake, with a marked gradient in the suboxic layer (Fig. 2C). Redox values (Eh) were high in the mixolimnion, and started to decline with increasing depth from 40 m down to 58 m, *i.e.*, the bottom of the suboxic zone (Fig. 2C). Suspended particulate matter (SPM) was quite homogenous and low in the mixolimnion, and increased markedly around the oxycline as well as at the bottom of the lake in the nepheloid layer (Busigny et al., 2014) up to 0.96 mg L^{-1} (Fig. 2D). DOC concentrations (Fig. 3A) averaged 90.4 ± 13.6 µmol L^{-1}, and increased gradually from the top of the monimolimnion up to 354 µmol L^{-1} at the bottom of the lake. POC concentrations increased in the mesolimnion from an average concentration of 11.5 ± 5 µmol L^{-1} in the mixolimnion to 21.4 ± 2 µmol L^{-1} in the monimolimnion. The high value at 90 m (~39 µmol L^{-1}) suggests that particles from the nepheloid layer were sampled. Total dissolved phosphates (TDP) were only measurable below 65 m depth and increased rapidly in the monimolimnion up to 0.5 mmol L^{-1} at 70 m depth. Particulate phosphorus (P_P) increased steadily from negligible values above 54 m (*i.e.*, above the oxycline), up to 0.3 mmol L^{-1} at the lake bottom (Fig. 3B).

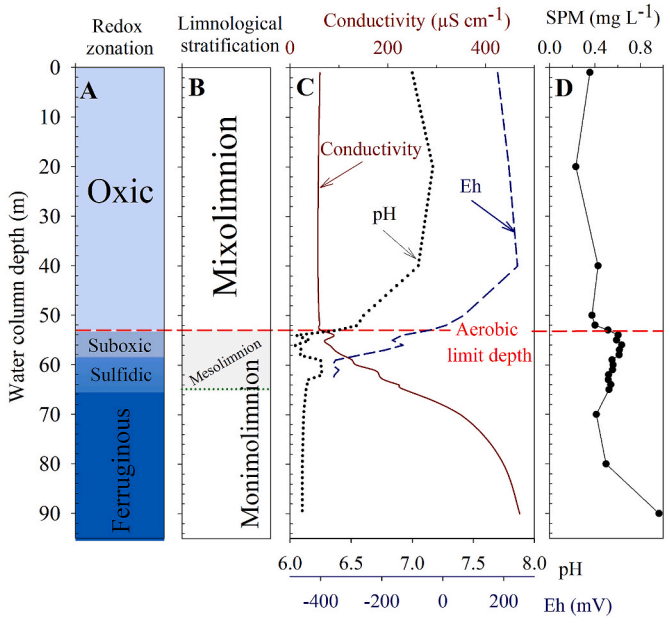

Fig. 2. Vertical zonation of Lake Pavin water column based on (A) redox domains, (B) water limnological stratification, (C) electrical conductivity, pH, redox potential (Eh), and (D) suspended particulate matter (SPM) concentrations measured in July 2018.

Consistent with the definitions by Froelich et al. (1979), Poulton and Canfield (2011), and Busigny et al. (2016), four redox zones were identified in the water column of Lake Pavin (Fig. 2A): (i) the oxic zone where molecular oxygen is still present (0–53 m); (ii) the suboxic zone without molecular oxygen, but where other electron acceptors, such as Fe^{III}, Mn^{IV}, or S^{VI}, are present (54–59 m); (iii) the sulfidic zone where the ΣH_2S is abundant (60–65 m); and (iv) the ferruginous layer where Fe^{II} prevails (65–90 m). Zone (i) belongs to the mixolimnion, zones (ii) and (iii) to the mesolimnion, and zone (iv) to the monimolimnion. Peaks of Fe_P and Mn_P are encountered above and at the interface between the oxic and suboxic layer, respectively, presumably because of precipitation of Fe and Mn diffusing upwards. There, neoformed oxy(hydr)oxides may have adsorbed dissolved organic matter and contribute to the POC peak. In the suboxic zone, Mn_P and Fe_P (Fig. 3C and D) started to decrease successively from 52 to 54 m depth, respectively. Consistently, dissolved Mn and Fe concentrations showed a mirrored increase in the form of reduced species as all dissolved Fe is found in its reduced form (Fe^{II}). The reduction of SO_4^{2-} started below 54 m, ΣH_2S appeared at 58 m and peaked up to 11 µmol L^{-1} around 62 m (Fig. 3E). It is worth mentioning that the sulfidic zone (zone with ΣH_2S) was identified between 58 and 65 m, i.e., overlapping the onset of the ferruginous zone.

These phase changes are also consistent with the conventional succession of redox biogeochemical reactions along the redox gradient, which trigger reductive dissolution of the oxy(hydr)oxides (Froelich et al., 1979), as already noticed in Lake Pavin by Viollier et al. (1997). Because of the limited amount of sulfur in the lake, ferruginous conditions set in the monimolimnion confers the singular characteristic to Lake Pavin (Bura-Nakic et al., 2009).

This ferruginous zone consists of anoxic conditions where Fe is mobilized as ferrous species (Fe^{II}), and was shown to be subsequently precipitated mainly as siderite and vivianite (Busigny et al., 2016; Cosmidis et al., 2014; Poulton and Canfield, 2011; Viollier et al., 1997). Near the bottom, the nepheloid layer comprises strong elemental concentration gradients that reflect the upward diffusion of dissolved ions from the surficial sediment (Busigny et al., 2014).

3.2. Mercury speciation profiles

Total Hg concentrations in Lake Pavin waters are in the picomolar range, one order of magnitude higher than the ultra-trace oceanic concentration range (Bowman et al., 2020), but similar to other pseudo-pristine lakes, *i.e.*, lakes without local anthropogenic Hg inputs (Guédron et al., 2017; Leermakers et al., 1996; Regnell et al., 1997). THg_F ranged from 0.4 to 8.8 pmol L^{-1} and THg_P from 0.4 to 4.6 pmol L^{-1}. Both THg_P and THg_F showed the lowest concentrations in the oxic mixolimnion and the highest ones in the mesolimnion (Fig. 4A).

THg_P concentrations reached their maxima at 57 m, whereas THg_F maximum was found below, at 59 m. Then, they both show a progressive downward decrease in the sulfidic zone of the mesolimnion (Fig. 4A). In the mixolimnion, THg_F represented ~50% of THg (i.e., THg_P + THg_F) and decreased abruptly to reach 27% at 55 m in the upper part of the

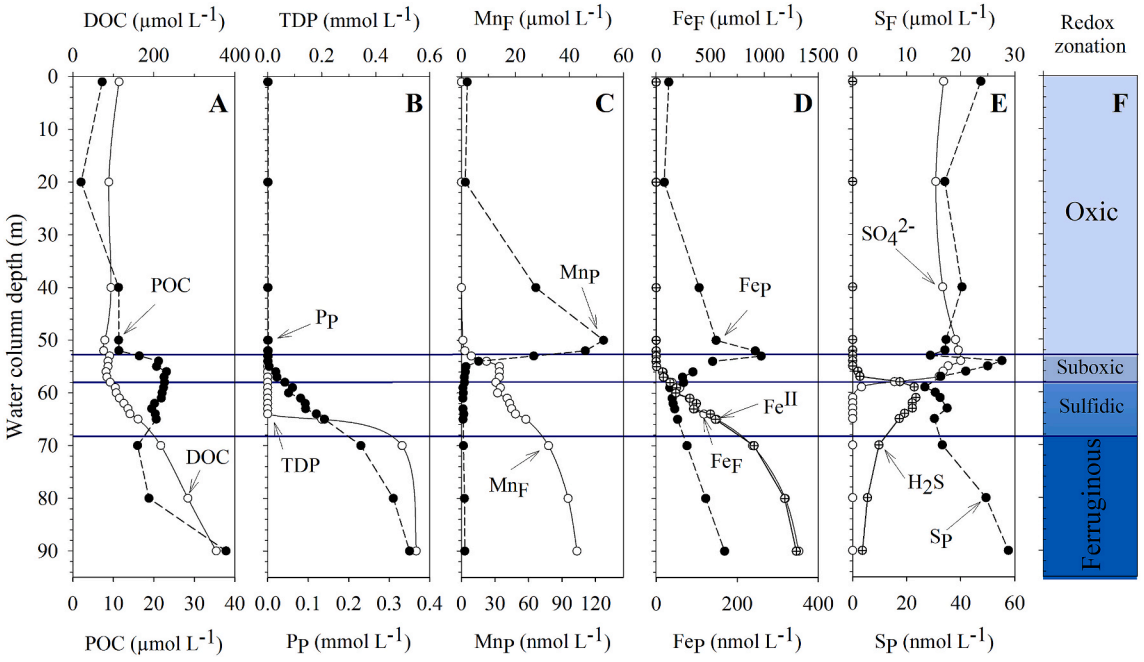

Fig. 3. Depth concentration profiles of dissolved and particulate (A) organic carbon, (B) phosphorus, (C) manganese, (D) iron, and (E) sulfur (sulfate, and sulfides) in the water column of Lake Pavin. Subscript F refers to filtered samples and subscript P to the particulate phase. The light blue band indicates the oxic zone, the light-dark blue band the suboxic zone, the blue one the sulfidic zone, and the dark blue band the Ferruginous zone. Fe^{II} is the reduced iron part of aqueous Fe (Fe_F). (For interpretation of the references to colour in this figure legend, the reader is referred to the Web version of this article.)

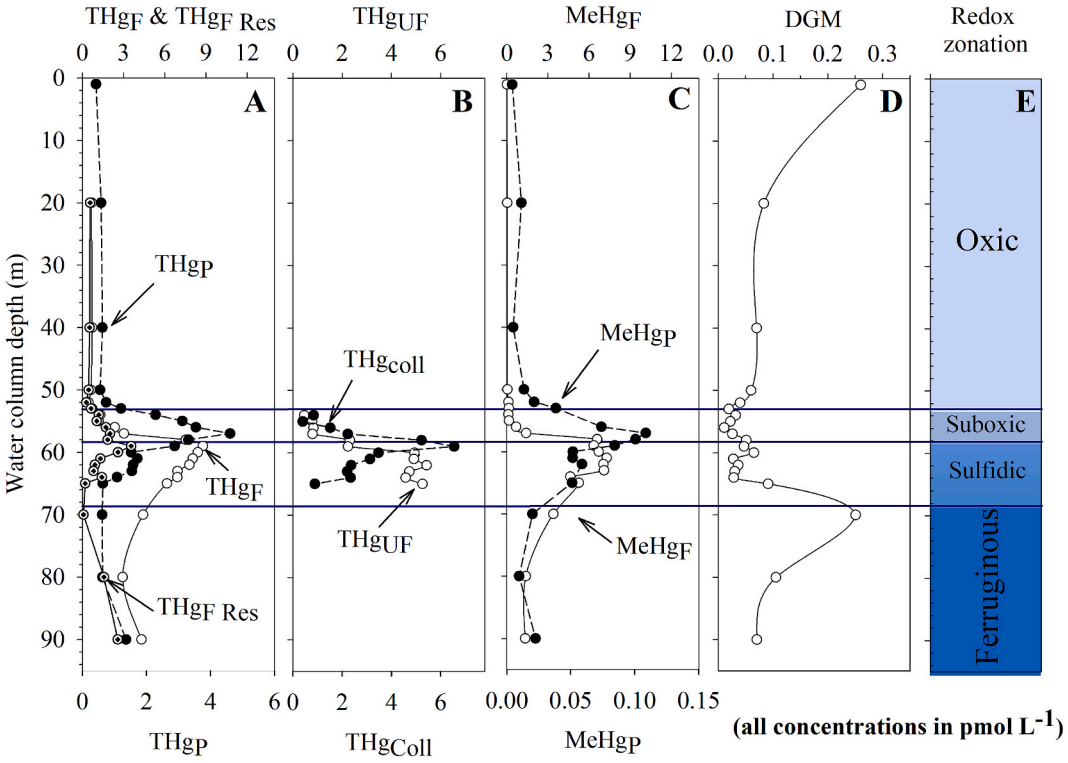

Fig. 4. Depth concentration profiles of filtered (upper X-axis) and particulate (bottom X-axis) fractions (A) total Hg filtrated (THg_F), particulate (THg_P) and residual Hg ($THg_{F\ Res} = THg_F - MeHg_F$), (B) ultra-filtered ($THg_{UF}$) and colloidal Hg ($THg_{coll}$), (C) dissolved gaseous Hg (DGM), and (D) methylmercury (MeHg). Corresponding redox zonation is also reported.

suboxic zone of the mesolimnion, followed by a gradual increase up to 75% at the bottom of this zone. Lateral advection of Hg from underground water inputs (few liters per second) present at mid-depth in the lake are negligible since a few measurements (data not shown) performed in the Goyon spring (45°30′34.7″ N; 2°54′15.6″ E) waters indicated THg and MeHg concentrations at the picomolar level. Below, in the sulfidic part of the mesolimnion, the proportion of the THg_F increased gradually to reach an average percentage of 85% of THg.

Within the filtered fraction, the "truly dissolved" THg (THg_{UF}: 0.5–5.4 pmol L^{-1}) and colloidal part of the THg_F (THg_{coll} = 0.4–6.5 pmol L^{-1}) were quantitatively comparable. In the suboxic zone, THg_{coll} presented a sharp peak at 59 m which dominated (i.e., 63 ± 15%) the THg_F fraction, and decreased in the sulfidic zone (32 ± 9% of THg_F) to the benefit of THg_{UF} (Fig. 4B). Noteworthy is that the maxima of the various THg fractions follow each other within a few meters between 57 and 60 m deepening from particulate, colloidal, <0.45 μm, and truly dissolved. This suggests a progressive dissolution of Hg downward.

$MeHg_F$ ranged from 0.03 to 6.8 pmol L^{-1}, whereas $MeHg_P$ concentrations were two orders of magnitude lower. Its distribution resembles the one of THg, with low concentration in the oxic mixolimnion and higher ones in the anoxic monimolimnion, where it reaches up to 7.1 pmol L^{-1} in the sulfidic zone of the lake (Fig. 4C). $MeHg_P$ peaked at 57 m whereas $MeHg_F$ showed a broader maximum between 58 and 63 m (Fig. 4C). $MeHg_F$ represented a minor fraction of THg_F in the oxic mixolimnion (<20%), and this proportion increased dramatically in the suboxic and anoxic monimolimnion, reaching 90% between 62 and 70 m, and then decreased below 40% at the bottom of the lake. Overall, $MeHg_F$, including the colloidal phase, is clearly the dominant Hg species in the sulfidic zone. In contrast, $MeHg_P$ never exceeded 10% of the THg_P with the highest proportions at 62 m.

Finally, DGM was between one and two order of magnitude lower than THg with the highest concentrations found at the surface (0.26 pmol L^{-1}) and in the middle of the monimolimnion (0.25 pmol L^{-1} at 70 m, Fig. 4C).

3.3. Crossed modeling using Wham 7 and PhreeqC 2.0

According to the thermodynamic calculations with Wham 7 and PhreeqC 2.0, in the mixolimnion, Hg and MeHg speciation is dominated by complexes with organic ligands (i.e., 98% for Hg-FA and up to 87% MeHg-FA of the total MeHg) (Fig. 5 A and B). However, when dissolved sulfide is present, in the sulfidic zone of the lake, complexes with sulfur ligands dominate (i.e., >65% of HgS and about 100% of MeHgSH). Calculated saturation indexes indicated the saturation of iron oxides, mostly hematite (Fe_2O_3) and goethite (FeOOH), in the suboxic part of the lake (Fig. 5C), whereas mineral phases of Fe, S, and P, including crystallized FeS (i.e., mackinawite) and vivianite ($Fe_3(PO_4)_2.8H_20$), are predicted to be saturated to over-saturated from the top of the sulfidic zone to the lake bottom (Fig. 5D).

These results are consistent with previously published data (Bura-Nakic et al., 2009; Busigny et al., 2016; Jézéquel et al., 2016; Viollier et al., 1997). Interestingly, cinnabar (alpha and beta) minerals were found to be saturated in the upper part of the sulfidic zone (Fig. 5D), while all other Hg mineral species tested (Tab. SI2), were found to be under-saturated.

4. Discussion

4.1. Mercury carrier-phase exchanges along the redox gradient

In oxic waters, potential solid Hg carrier phases are limited due to the low mineralogical diversity of SPM in the upper part of Lake Pavin (Miot et al., 2016). In surface waters, the biogenic particulate matter, mainly composed of diatoms and bacteria (Amblard and Bourdier, 1990; Miot et al., 2016), constitutes the sink for atmospheric Hg deposited onto the surface of the lake. Known as the "biological pump" (Hain et al., 2014), this process is common for removing trace elements (including Hg) from surface waters of oceans and lakes, especially when it contains diatoms (Zaferani et al., 2018). This interpretation is supported by the positive relationship between THg_P and POC in the mixolimnion (R^2 = 0.75, Fig. 6A). THg_P is also found correlated with Fe_P (R^2 = 0.90, Fig. 6A) which suggest a possible implication of the Fe oxides in the Hg-particulate organic matter (POM) consortiums. THg_F in the mixolimnion is also correlated with DOC (Fig. 6B), consistently with the predictions of our modeling, which shows that Hg-FA complexes dominate Hg species (98%) in the filtered phase (Fig. 5). The Hg-DOC association in natural waters is often thought to be the result of the high affinity of Hg for thiol functional groups of the DOC (Bouchet et al., 2018; Haitzer et al., 2002; Skyllberg et al., 2003).

The vertical downward POM flux is slowed down when reaching the density gradient in the mesolimnion and accumulated as indicated by the increase of THg, POC and SPM. There, POM feeds the heterotrophic microorganisms, resulting in dissolved O_2 consumption as previously described by Michard et al. (1994).

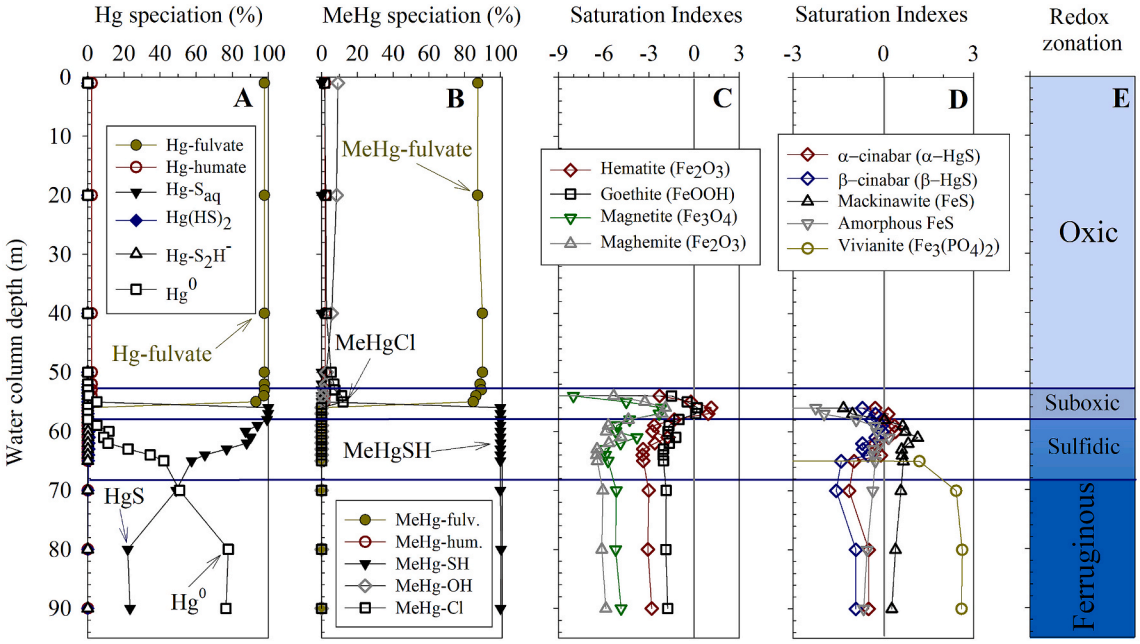

Fig. 5. Modeled (A) Hg speciation (= THg-MeHg) including Hg^{II} and Hg^0 species, (B) MeHg speciation, and saturation indexes for (C) iron oxy(hydr)oxides and (D) sulfide and vivianite minerals (WHAM 7.0 and PHREEQC 2.0). Pyrrhotite saturation index was below −100 and is not presented in the figure. Corresponding redox zonation is also reported.

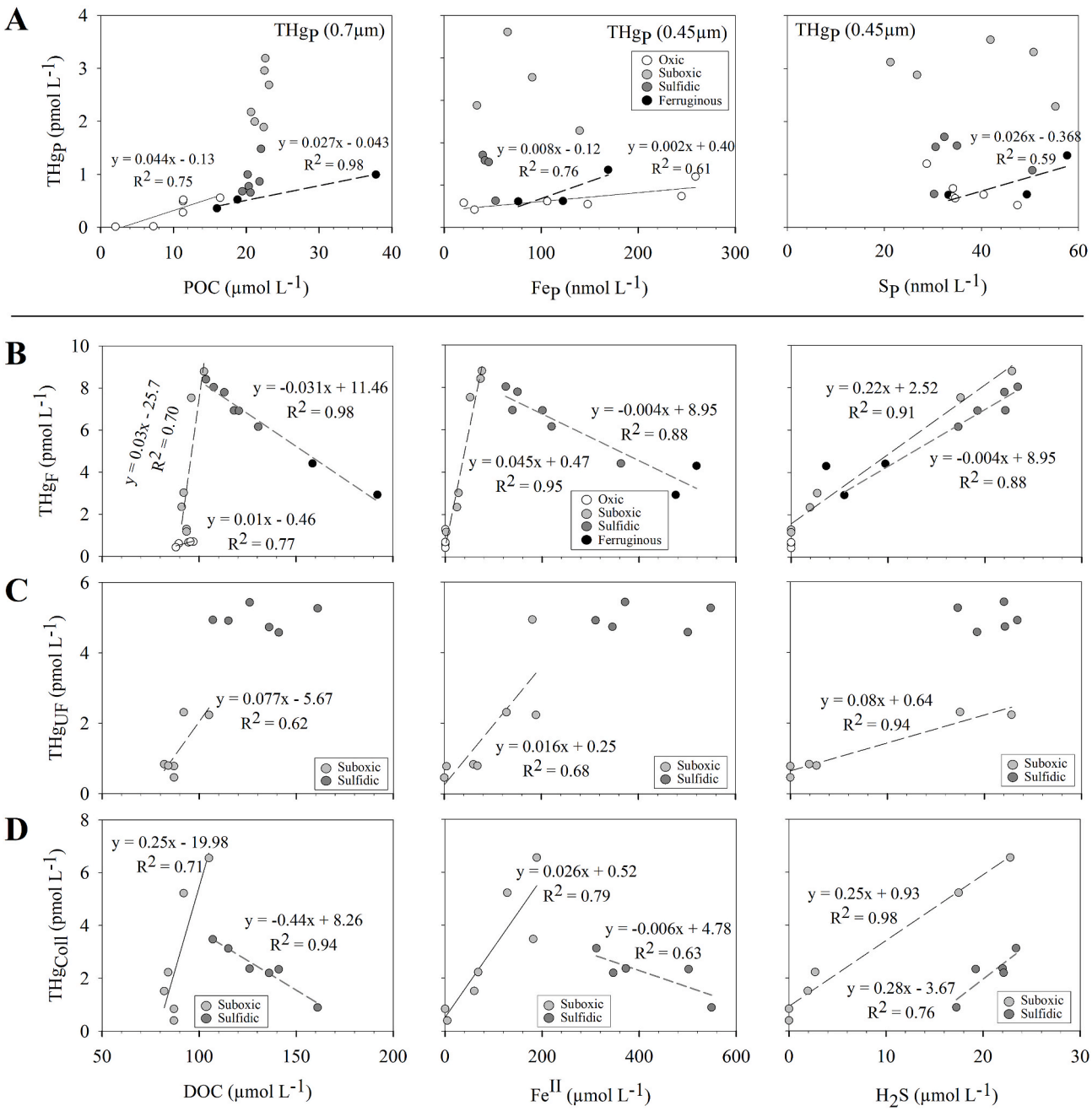

Fig. 6. Total Mercury concentration in the A) the particulate (THg_P), B) the filtered (THg_F <0.45 µm), C) the truly dissolved (THg_{UF}), and D) the colloidal (THg_{coll}) fractions versus organic carbon, iron and sulfide in the particulate (A) and filtered (B to D) fractions. Left panel of plot A reports particulate mercury (THg_P) and organic carbon (POC) obtained from the digestion of 0.7 µm (GF/F) filters. Central and right panels report particulate mercury (THg_P), iron (Fe_P) and sulfur (S_P) concentrations obtained from the digestion of 0.45 µm (PTFE) filters. All plotted regressions are significant and have p values below 0.05.

In the mesolimnion, no significant correlation was found between THg_P and POC, nor with concentration of particulate Fe or S. This likely reflects the recycling of Hg onto successive neoformed phases along the redox gradient (i.e., POC mineralization, reductive dissolution of Mn and Fe oxy(hydr)oxides, Cf section 3.1). Changes in Hg carrier phases is particularly evident in the filtered phase, as peaks in THg_F and $MeHg_F$ occur below the onset of the decay of both THg_P and $MeHg_P$, i.e., from the boundary between suboxic and sulfidic zone (Fig. 4). Consistently with the recycling of POC and Mn or Fe oxides, both the truly dissolved Hg (THg_{UF}) and the colloidal Hg (THg_{coll}) are found positively correlated with DOC, Fe^{II} and ΣH_2S in the suboxic zone (Fig. 6 C and D). This confirms that the mineralization of POM and the reductive dissolution of Fe-oxy(hydr)oxides below the oxycline have resulted in the release of dissolved Hg and Fe^{II} (Hellal et al., 2015), and their redistribution in the filtered fraction, with a dominance of Hg species bound to OM and/or FeS (i.e., mackinawite, Fig. 5D) colloids (THg_{coll} = 63 ± 15% of THg_F). Below, in the sulfidic mesolimnion, our modeling predicted the formation of both α- and β-cinnabar and FeS mineral phases (*i.e.*, mackinawite and other amorphous FeS phases, Fig. 5D) consistently with previous studies (Bura-Nakic et al., 2009). In the filtered phase, truly dissolved THg (THg_{UF} = 68 ± 9% of THg_F) becomes dominant, and is found independent of DOC, Fe^{II} and ΣH_2S (Fig. 6C). In contrast, THg_F and THg_{coll} are inversely correlated with DOC and Fe^{II}, but positively correlated with ΣH_2S (Fig. 6 B and D). This most probably illustrates the complex formation of Hg with sulfides in solution (*i.e.*, HgS nanoparticles and/or dissolved Hg-polysulfides) at the expense of OM complexation as

confirmed by our model (Fig. 5A and B), and consistently with colloidal HgS identified by Energy dispersive X-ray spectrometry in deep-water of the Lake Pavin (Miot et al., 2016). Although the thermodynamic modeling does not allow modeling colloidal HgS, the model predicts the precipitation of HgS particles at the top of the sulfidic mesolimnion (Fig. 5D). Hence, during the degradation of the POM in suboxic and anoxic conditions, the nature of the particulate Hg-OM binding sites change, favoring the preferential binding of Hg to stronger dissolved ligands, such as thiol groups of the FA (Bouchet et al., 2018; Feyte et al., 2012; Liang et al., 2019) and the formation of FeS and HgS colloids in the dissolved phase, which is at equilibrium with HgS minerals.

In the ferruginous monimolimnion, although the number of observations is limited (n = 3), THg_P rise with rising POC, Fe_P and S_P concentrations (Fig. 6A). This is consistent with an association of Hg with both iron sulfides, and/or sulfidized OM, consistent with the predictions of the model. It is however important to recall that this area is the most devoid of particulate Hg. In this ferruginous zone, Fe_P and P_P covary ($R^2 = 0.95$, n = 3, $p < 0.10$), with 1.5 mol of Fe per mole of P, supporting the presence of vivianite as already identified in deep waters of Lake Pavin (Busigny et al., 2016; Cosmidis et al., 2014) and confirmed by our thermodynamic modeling (Fig. 5D). It is thus probable that such Fe-phosphates precipitates together with other FeS minerals, in association with bacteria (Miot et al., 2016) or diatoms (i.e., THg_P *vs* Si_P, $R^2 = 0.64$, n = 6, $p < 0.05$), could favor the scavenging and export of Hg to the sediment of Lake Pavin. In brief, the Hg-OM partition appears to be involved in the Fe–S redox and partition changes known as the "iron--wheel" of the Lake Pavin (Busigny et al., 2016; Viollier et al., 1997).

4.2. Mercury methylation/demethylation

MeHg in Lake Pavin is in similar proportions as in other meromictic lakes or artificial reservoirs in various lakes around the world (Peretyazhko et al., 2006b; Watras and Bloom, 1994). In the Great Salt Lake, the Petit-Saut reservoir, and Wisconsin or Canadian lakes, all stratified with an anoxic hypolimnion, comparable MeHg distribution patterns have been observed resulting from increased net Hg methylation in the lake bottom waters (Achá et al., 2012; Eckley et al., 2005; Eckley and Hintelmann, 2006; Muresan et al., 2008; Porcella, 1994; Regnell et al., 1997; Regnell and Tunlid, 1991; Watras and Bloom, 1994; Yang et al., 2020). The same is true for marine environments where meromixis occurs (e.g., Black Sea and the Baltic Sea), resulting in high MeHg in their anoxic waters (Pempkowiak et al., 1998; Rosati et al., 2018; Soerensen et al., 2018).

In Lake Pavin, MeHg is strongly correlated with THg both in the filtered phase ($R^2 = 0.92$, n = 21, $p < 0.01$), and in the particulate phase ($R^2 = 0.85$, n = 21, $p < 0.01$). In the monimolimnion, MeHg constitutes the main fraction of the THg (*i.e.*, 77 ± 22% of the THg_F, and 71 ± 24% of the THg_P). $MeHg_F$ is highly correlated with ΣH_2S ($R^2 = 0.96$, n = 20, $p < 0.01$) along the entire water column. The onset of MeHg accumulation occurs in the suboxic zone, and reaches a plateau in the sulfidic layer where ΣH_2S and Fe^{II} are the most intensively produced. The steepest $MeHg_F$ gradient is located between 57 and 58 m (Fig. 4D), at the same depth as the steepest $SO_4/\Sigma H_2S$ drops (Fig. 3D and E). This feature indicates that MeHg is dominantly produced by methylating-SRB, a group of strains reported owning the methylating *hgc* gene (Paranjape and Hall, 2017; Regnell and Watras, 2018). SRB account for a large part of the bacteria in the entire monimolimnion of Lake Pavin (Berg et al., 2019; Lehours et al., 2016). The presence of high $MeHg_F$ and THg_{UF} ($R^2 = 0.84$, n = 12, $p < 0.01$) concentrations in the sulfidic zone (Fig. 4B and D) strongly suggests that HgS complexes, neutral Hg polysulfides, and possibly Hg-thiolates (Fig. 5A and B), are abundant enough to constitute substrates for Hg methylation by SRB as suggested in several experiments or modeling (Benoit et al., 1999; Schaefer and Morel, 2009; Skyllberg, 2008). On the other hand, several strains can demethylate MeHg under anoxic conditions including SRB and methanogens (Bridou et al., 2011; Oremland et al., 1991). The decrease in $MeHg_F$ concentrations in the ferruginous zone is coincident with the increase in DGM, which supports the hypothesis of reductive demethylation in the Lake bottom. However, the amount of produced DGM could only explain a small fraction (i.e. <5–10%) of the decrease of MeHgF observed, suggesting that significant proportion of $MeHg_F$ is also likely exported to the sediment in association neoformed FeS minerals (see paragraph 5.1.).

4.3. Mercury reduction

The DGM concentration profile in the Lake Pavin waters column exhibits high levels in surface waters and at 70 m in the anoxic monimolimnion (Fig. 4C). No trace of dimethylmercury was found in the samples, consistently with previous results (Cossa et al., 1994), suggesting that DGM consists entirely of Hg^0. The high DGM measured in surface waters suggests that Hg^0 is formed via Hg^{II} photoreduction in the euphotic zone, and is partially reinjected in the atmosphere as already shown in numerous lakes (Amyot et al., 1994; Guédron et al., 2020a; Saiz-Lopez et al., 2018). In contrast, the presence of DGM peaks in the aphotic monimolimnion supports non-photochemical processes for DGM production, such as Hg^{II} microbial reduction (Lamborg et al., 2013; Mason et al., 1995; Rolfhus and Fitzgerald, 2004) and/or natural OM-mediated reduction of Hg^{II} (Allard and Arsenie, 1991; Zheng et al., 2011). Hg^0 is consistently predicted by the model, increasing from the sulfidic mesolimnion to the ferruginous monimolimnion (Fig. 5A). The large proportion of truly dissolved Hg (i.e., 59 and 81% of THg_F) possibly bound to labile organic molecules could favor its reduction by natural OM (Gu et al., 2011; Zheng et al., 2011). Alternatively, the abiotic reduction of Hg^{II} to Hg^0 could also be induced by Fe^{II} in the presence of Fe-oxy(hydr)oxides (Charlet et al., 2002; Peretyazhko et al., 2006a), such as hematite reported from 70 m down to 86 m in the Pavin Lake (Cosmidis et al., 2014). Hg reduction in the presence of nanoparticulate vivianite has also recently been demonstrated in anoxic circumneutral pH water (Etique et al., 2021). Also, the reduction of Hg^{II}-S^{-II} complexes by FeS to Hg^0 is thermodynamically possible (Bone et al., 2014) at Eh values in the range of Lake Pavin waters below 59 m. However, the occurrence of DGM peaks in the monimolimnion in phase with decreasing MeHg concentrations (Fig. 4) also supports the hypothesis of reductive MeHg demethylation with the production of Hg^0 and CH_4 (Aeschbach-Hertig et al., 1999). Reductive demethylation is the fact of *Geobacter* sp. (Lu et al., 2016), some of them identified in Lake Pavin waters (Berg et al., 2019). In summary, under the current observations of Pavin waters, it is not possible to sort out the actual reactions involved in the reducing process that produce the DGM in the monimolimnion. In the present state, we cannot explain the difference between the measured and model-derived DGM concentrations. An in-depth study with higher resolution lake bottom profiles together with experimental works are required to solve this issue.

5. Synthesis and conclusions

The high-resolution observation and modeling of Hg speciation and partition at the redox interfaces of Lake Pavin allow the proposal of a conceptual biogeochemical behavior of Hg which can be typical of other meromictic ferruginous lakes (Fig. 7). Because it has a very small catchment area that minimizes Hg inputs from the drainage basin, Lake Pavin receives Hg mainly from the atmosphere. Once deposited onto surface waters, a part of Hg is photo-reduced and reinjected in the atmosphere, whereas another part binds to DOC and sorbs onto biogenic particulate matter produced in the euphotic zone and conveyed at depth by settling POC, in a process known as "biological pumping".

The Hg associated with POM accumulates where the conductivity gradient generates a strong stratification. There, the mineralization of OM occurs, consuming dissolved oxygen and generating a suboxic zone, causing the mobilization of a fraction of Hg. Mercury diffuses up and down from this Hg-enriched zone. On its way up, Hg adsorbs onto Fe-oxy

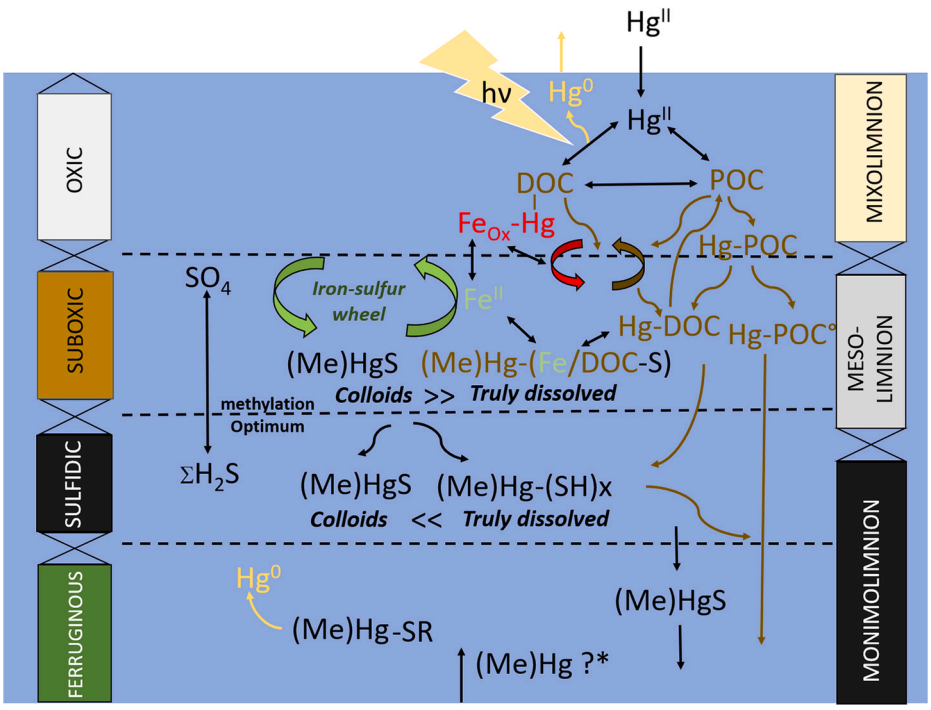

Fig. 7. Conceptual model for the Hg and MeHg cycle in Lake Pavin with the recycling of organic matter, sulfur, and iron. (Me)Hg refers to both MeHg and Hg species, ticks (-) indicate the binding with particulate carrier phases (i.e., iron oxides (Fe_{Ox}), particulate organic carbon (POC) and iron sulfides (FeS) or binding with aqueous ligands (i.e., dissolved organic carbon (DOC), free or DOC polysulfides (SR). Hg-POC° considers Hg bound to both particles and microbial cells. (Me)Hg* refers to possible upward release of MeHg and THg from the sediment.

(hydr)oxides (associated with POM) that precipitated on the top of the oxycline; on its way down, Hg diffuses as truly-dissolved and colloidal HgS species and partly precipitate as HgS minerals. Simultaneously, in this suboxic zone, available Hg^{II} is methylated by SRB. Deeper in the anoxic monimolimnion, sulfidation favors the formation of dissolved Hg fraction and possibly the reductive demethylation of MeHg with Hg^0 production. A part of the Hg and MeHg produced in the suboxic and sulfidic zone is also likely exported to the sediment with settling particles. In brief, the "biological pump", the "iron-sulfur wheel", through associated bacteria consortia, control the Hg cycling in the Pavin waters. This behavior is in line with already existing biogeochemical models and allows us to observe the already identified homogenous and heterogeneous reactions and processes along a single water column covering the entire redox range of natural waters. More detailed observations on the Hg speciation in the ferruginous monimolimnion are needed to evaluate the possible effect of Hg input from hydrothermal and diffusive inputs at the bottom of the lake in addition to quantitative export fluxes and reaction rates within the lake.

Declaration of competing interest

The authors declare the following financial interests/personal relationships which may be considered as potential competing interests: Guedron reports financial support was provided by French National Research Agency.

Data availability

Data will be made available on request.

Acknowledgments

All chemical analyses have been performed at the *Geochemistry & Mineralogy* platform of ISTerre (Université Grenoble Alpes, France), except for particulate organic carbon that has been determined at the analytical platform of the Mediterranean Institute of Oceanography (MIO, Université Aix-Marseille, France), and anions that have been determined at the Air-o-sol analytical platform of the Institute of Environmental Geosciences (IGE, Université Grenoble Alpes, France). This work is a contribution to the PALMERLAC project supported by a grant from Labex OSUG@2020 (PI: D. Cossa and D. Tisserand). D. Cossa, D. Tisserand, and S. Guédron (ISTerre/IRD/UGA) are part of Labex OSUG@2020 (Investissements d'avenir ANR10 LABX56). The authors thank the City of Besse-et-Saint-Anastaise and the members of the Station Biologique de Besse (Université Clermont Auvergne), especially Corinne Mesta for logistical supports during field campaigns, and colleagues from IPGP and IMPMC for their help during sampling.

Appendix A. Supplementary data

Supplementary data to this article can be found online at https://doi.org/10.1016/j.apgeochem.2022.105463.

References

Achá, D., Pabon, C.A., Hintelmann, H., 2012. Mercury methylation and hydrogen sulfide production among unexpected strains isolated from periphyton of two macrophytes of the Amazon. FEMS Microbiol. Ecol. 80, 637–645.

Aeschbach-Hertig, W., Hofer, M., Kipfer, R., Imboden, D., Wieler, R., 1999. Accumulation of mantle gases in a permanently stratified volcanic Lake (Lac Pavin, France). Geochem. Cosmochim. Acta 63, 3357–3372.

Amblard, C., Bourdier, G., 1990. The spring bloom of the diatom Melosira italica subsp. subarctica in Lake Pavin: biochemical, energetic and metabolic aspects during sedimentation. J. Plankton Res. 12, 645–660.

Amyot, M., McQueen, D.J., Mierle, G., Lean, D.R.S., 1994. Sunlight-induced formation of dissolved gaseous mercury in Lake waters. Environ. Sci. Technol. 28, 2366–2371.

Barone, V., Bencini, A., Totti, F., Uytterhoeven, M.G., 1996. Theoretical characterization of the mechanism of Hg– C bond cleavage by halogenic acids. Organometallics 15, 1465–1469.

Benoit, J., Gilmour, C., Mason, R., Heyes, A., 1999. Sulfide controls on mercury speciation and bioavailability to methylating bacteria in sediment pore waters. Environ. Sci. Technol. 33, 951–957.

Berg, J.S., Jézéquel, D., Duverger, A., Lamy, D., Laberty-Robert, C., Miot, J., 2019. Microbial diversity involved in iron and cryptic sulfur cycling in the ferruginous, low-sulfate waters of Lake Pavin. PLoS One 14, e0212787.

Blanc, P., Burnol, A., Marty, N., Hellal, J., Guérin, V., Laperche, V., 2018. Methylmercury complexes: selection of thermodynamic properties and application to the modelling of a column experiment. Sci. Total Environ. 621, 368–375.

Bloom, N., 1996. Method 1613 Mercury in Water by Oxidation, Purge, and Trap. CVAFS, Washington.

Bone, S.E., Bargar, J.R., Sposito, G., 2014. Mackinawite (FeS) reduces mercury (II) under sulfidic conditions. Environ. Sci. Technol. 48, 10681–10689.

Bonhomme, C., Jézéquel, D., Poulin, M., Saad, M., Vinçon-Leite, B., Tassin, B., 2016. Lake Pavin Mixing: New Insights from High Resolution Continuous Measurements. Springer, Lake Pavin, pp. 177–184.
Bonhomme, C., Poulin, M., Vinçon-Leite, B., Saad, M., Groleau, A., Jézéquel, D., Tassin, B., 2011. Maintaining meromixis in Lake Pavin (Auvergne, France): the key role of a sublacustrine spring. Compt. Rendus Geosci. 343, 749–759.
Bouchet, S., Goni-Urriza, M., Monperrus, M., Guyoneaud, R., Fernandez, P., Heredia, C., Tessier, E., Gassie, C., Point, D., Guédron, S., Acha, D., Amouroux, D., 2018. Linking microbial activities and low molecular weight thiols to Hg methylation in biofilms and periphyton from high altitude tropical lakes (Bolivian altiplano). Environ. Sci. Technol. 52, 9758–9767.
Bowman, K.L., Lamborg, C.H., Agather, A.M., 2020. A global perspective on mercury cycling in the ocean. Sci. Total Environ. 710, 136166.
Bridou, R., Monperrus, M., Gonzalez, P.R., Guyoneaud, R., Amouroux, D., 2011. Simultaneous determination of mercury methylation and demethylation capacities of various sulfate-reducing bacteria using species-specific isotopic tracers. Environ. Toxicol. Chem. 30, 337–344.
Buffle, J., Chalmers, R.A., 1988. Complexation reactions in aquatic systems. Ellis Norwood Ltd., Chichester, p. 692. Chichester (1988).
Bura-Nakic, E., Viollier, E., Jézéquel, D., Thiam, A., Ciglenecki, I., 2009. Reduced sulfur and iron species in anoxic water column of meromictic crater Lake Pavin (Massif Central, France). Chem. Geol. 266, 311–317.
Busigny, V., Jézéquel, D., Cosmidis, J., Viollier, E., Benzerara, K., Planavsky, N.J., Albéric, P., Lebeau, O., Sarazin, G., Michard, G., 2016. The Iron Wheel in Lac Pavin: Interaction with Phosphorus Cycle, Lake Pavin. Springer, pp. 205–220.
Busigny, V., Mathon, F.P., Jézéquel, D., Bidaud, C.C., Viollier, E., Bardoux, G., Bourrand, J.j., Benzerara, K., Duprat, E., Menguy, N., 2022. Mass collection of magnetotactic bacteria from the permanently stratified ferruginous Lake Pavin, France. Environ. Microbiol. 24, 721–736.
Busigny, V., Planavsky, N.J., Jézéquel, D., Crowe, S., Louvat, P., Moureau, J., Viollier, E., Lyons, T.W., 2014. Iron isotopes in an Archean ocean analogue. Geochem. Cosmochim. Acta 133, 443–462.
Chapron, E., Albéric, P., Jézéquel, D., Versteeg, W., Bourdier, J.-L., Sitbon, J., 2010. Multidisciplinary characterisation of sedimentary processes in a recent maar lake (Lake Pavin, French Massif Central) and implication for natural hazards. Nat. Hazards Earth Syst. Sci. 10, 1815–1827.
Charlet, L., Bosbach, D., Peretyashko, T., 2002. Natural attenuation of TCE, AS, Hg linked to the heterogeneous oxidation of Fe (II) : an AFM study. Chem. Geol.
Cline, J.D., 1969. Spectrophotometric determination of hydrogen sulfide in natural waters 1. Limnol. Oceanogr. 14, 454–458.
Cooper, C.J., Zheng, K., Rush, K.W., Johs, A., Sanders, B.C., Pavlopoulos, G.A., Kyrpides, N.C., Podar, M., Ovchinnikov, S., Ragsdale, S.W., Parks, J.M., 2020. Structure determination of the HgcAB complex using metagenome sequence data: insights into microbial mercury methylation. Communications Biology 3, 320.
Cosmidis, J., Benzerara, K., Morin, G., Busigny, V., Lebeau, O., Jézéquel, D., Noël, V., Dublet, G., Othmane, G., 2014. Biomineralization of iron-phosphates in the water column of lake Pavin (Massif central, France). Geochem. Cosmochim. Acta 126, 78–96.
Cossa, D., Averty, B., Bretaudeau, J., Senard, A.S., 2003. Dissolved Mercury Speciation in Marine Waters. Analysis Methods in Marine Environment. Ifremer and French Ministry of Sustainable Development and Ecology (in French).
Cossa, D., Coquery, M., 2005. The mediterranean mercury anomaly, a geochemical or a biologocalissue. The Mediterranean Sea 177–208.
Cossa, D., de Madron, X.D., Schaefer, J., Guédron, S., Marusczak, N., Castelle, S., Naudin, J.-J., 2017. Sources and exchanges of mercury in the waters of the Northwestern Mediterranean margin. Prog. Oceanogr.
Cossa, D., Gobeil, C., 2000. Mercury speciation in the lower st. Lawrence estuary. Can. J. Fish. Aquat. Sci. 57, 138–147.
Cossa, D., Mason, R.P., Fitzgerald, W.F., 1994. Chemical speciation of mercury in a Meromictic lake. In: W C, J., H J, W. (Eds.), Mercury Pollution: Integration and Synthesis. CRC Press, Inc., pp. 57–67
Drott, A., Björn, E., Bouchet, S., Skyllberg, U., 2013. Refining thermodynamic constants for mercury(II)-Sulfides in equilibrium with metacinnabar at sub-micromolar aqueous sulfide concentrations. Environ. Sci. Technol. 47, 4197–4203.
Dyrssen, D., Wedborg, M., 1991. The sulphur-mercury(II) system in natural waters. Water Air Soil Pollut. 56, 507–519.
Eckley, C., Watras, C., Hintelmann, H., Morrison, K., Kent, A., Regnell, O., 2005. Mercury methylation in the hypolimnetic waters of lakes with and without connection to wetlands in northern Wisconsin. Can. J. Fish. Aquat. Sci. 62, 400–411.
Eckley, C.S., Hintelmann, H., 2006. Determination of mercury methylation potentials in the water column of lakes across Canada. Sci. Total Environ. 368, 111–125.
Etique, M., Bouchet, S., Byrne, J.M., ThomasArrigo, L.K., Kaegi, R., Kretzschmar, R., 2021. Mercury Reduction by Nanoparticulate Vivianite. Environmental Science & Technology.
Feyte, S., Gobeil, C., Tessier, A., Cossa, D., 2012. Mercury dynamics in lake sediments. Geochem. Cosmochim. Acta 82, 92–112.
Feyte, S., Tessier, A., Gobeil, C., Cossa, D., 2010. In situ adsorption of mercury, methylmercury and other elements by iron oxyhydroxides and organic matter in lake sediments. Appl. Geochem. 25, 984–995.
Fitzgerald, W.F., Lamborg, C.H., Turekian, H.D., Holland, K.K., 2014. 11.4 - Geochemistry of mercury in the environment. In: Treatise on Geochemistry, second ed. Elsevier, Oxford, pp. 91–129.
Froelich, P.N., Klinhammer, G.P., Bender, M.L., Luedtke, N.A., Heath, G.R., Cullen, D., Dauphin, P., Hammond, D., Hartman, B., Maynard, V., 1979. Early oxidation of organic matter in pelagic sediments of the eastern equatorial atlantic: suboxic diagenesis. Geochemica et cosmochemica Acta 43, 1075–1090.
Gobeil, C., Cossa, D., 1993. Mercury in sediments and sediment pore water in the Laurential Trough. Can. J. Fish. Aquat. Sci. 50, 1794–1880.
Gu, B., Bian, Y., Miller, C.L., Dong, W., Jiang, X., Liang, L., 2011. Mercury reduction and complexation by natural organic matter in anoxic environments. Proc. Natl. Acad. Sci. USA 108, 1479–1483.
Guédron, S., Achá, D., Bouchet, S., Point, D., Tessier, E., Heredia, C., Rocha-Lupa, S., Fernandez-Saavedra, P., Flores, M., Bureau, S., 2020a. Accumulation of methylmercury in the high-altitude lake uru uru (3686 m asl, Bolivia) controlled by sediment efflux and photodegradation. Appl. Sci. 10, 7936.
Guédron, S., Audry, S., Acha, D., Bouchet, S., Point, D., Condom, T., Heredia, C., Campillo, S., Baya, P.A., Groleau, A., Amice, E., Amouroux, D., 2020b. Diagenetic production, accumulation and sediment-water exchanges of methylmercury in contrasted sediment facies of Lake Titicaca (Bolivia). Sci. Total Environ. 723, 138088.
Guédron, S., Devin, S., Vignati, D.A.L., 2016. Total and methylmercury partitioning between colloids and true solution: from case studies in sediment overlying and porewaters to a generalized model. Environ. Toxicol. Chem. 35, 330–339.
Guédron, S., Grimaldi, M., Grimaldi, C., Cossa, D., Tisserand, D., Charlet, L., 2011. Amazonian former gold mined soils as a source of methylmercury: evidence from a small scale watershed in French Guiana. Water Res. 45, 2659–2669.
Guédron, S., Point, D., Acha, D., Bouchet, S., Baya, P.A., Molina, C.I., Tessier, E., Monperrus, M., Flores, M., Fernandez Saavedra, P., Espinoza, M.E., Heredia, C., Rocha, S., Groleau, A., Amice, E., Thebault, J., Alanoca, L., Duwig, C., Uzu, G., Lazzaro, X., Bertrand, A., Bertrand, S., Barbaud, C., Gibon, F.M., Ibanez, C., Zepita, C., Chauvaud, L., Amouroux, D., 2017. Mercury contamination level and speciation inventory in the hydrosystem of Lake Titicaca: current status and future trends. Environ. Pollut. 231, 262–270.
Hain, M.P., Sigman, D., Haug, G., 2014. 8.18–The biological pump in the past. In: Reference Module in Earth Systems and Environmental Sciences Treatise on Geochemistry The Oceans and Marine Geochemistry, second ed., vol. 8, pp. 485–517.
Haitzer, M., Aiken, G.R., Ryan, J.N., 2002. Binding of mercury(II) to dissolved organic matter: the role of the mercury-to-DOM concentration ratio. Environ. Sci. Technol. 36, 3564–3570.
Hellal, J., Guédron, S., Huguet, L., Schaefer, J., Laperche, V., Joulian, C., Lanceleur, L., Burnol, A., Ghestem, J.-P., Garrido, F., Battaglia-Brunet, F., 2015. Mercury mobilization and speciation linked to bacterial iron oxide and sulfate reduction: a column study to mimic reactive transfer in an anoxic aquifer. J. Contam. Hydrol. 180, 56–68.
Iverfeldt, Å., 1988. Mercury in the Norwegian fjord framvaren. Mar. Chem. 23, 441–456.
Jeong, H.Y., Klaue, B., Blum, J.D., Hayes, K.F., 2007. Sorption of mercuric ion by synthetic nanocrystalline mackinawite (FeS). Environ. Sci. Technol. 41, 7699–7705.
Jézéquel, D., Michard, G., Viollier, E., Agrinier, P., Albéric, P., Lopes, F., Abril, G., Bergonzini, L., 2016. Carbon Cycle in a Meromictic Crater Lake: Lake Pavin, France, Lake Pavin. Springer, pp. 185–203.
Juvigné, E., Bastin, B., Delibrias, G., Evin, J., Gewelt, M., Gilot, E., Streel, M., 1996. A comprehensive pollen-and tephra-based chronostratigraphic model for the Late Glacial and Holocene period in the French Massif Central. Quat. Int. 34, 113–120.
Kim, C., Rytuba, J.J., Brown, J.G.E., 2004. EXAFS study of mercury (II) sorption to Fe- and Al- (hydr)oxides I. Effect of pH. J. Colloid Interface Sci. 271, 1–15.
Lamborg, C.H., Kent, D.B., Swarr, G.J., Munson, K.M., Kading, T., O'Connor, A.E., Fairchild, G.M., LeBlanc, D.R., Wiatrowski, H.A., 2013. Mercury speciation and mobilization in a wastewater-contaminated groundwater plume. Environ. Sci. Technol. 47, 13239–13249.
Lamborg, C.H., Yigiterhan, O., Fitzgerald, W.F., Balcom, P.H., Hammerschmidt, C.R., Murray, J., 2008. Vertical distribution of mercury species at two sites in the Western Black Sea. Mar. Chem. 111, 77–89.
Leermakers, M., Meuleman, C., Baeyens, W., 1996. Mercury Distribution and Fluxes in Lake Baikal, Global and Regional Mercury Cycles: Sources, Fluxes and Mass Balances. Springer, pp. 303–315.
Lehours, A.-C., Borrel, G., Morel-Desrosiers, N., Bardot, C., Grossi, V., Keraval, B., Attard, E., Morel, J.-P., Amblard, C., Fonty, G., 2016. Anaerobic Microbial Communities and Processes Involved in the Methane Cycle in Freshwater Lakes-A Focus on Lake Pavin, Lake Pavin. Springer, pp. 255–284.
Liang, X., Lu, X., Zhao, J., Liang, L., Zeng, E.Y., Gu, B., 2019. Stepwise reduction approach reveals mercury competitive binding and exchange reactions within natural organic matter and mixed organic ligands. Environ. Sci. Technol. 53, 10685–10694.
Lopes, F., Viollier, E., Thiam, A., Michard, G., Abril, G., Groleau, A., Prévot, F., Carrias, J.-F., Albéric, P., Jézéquel, D., 2011. Biogeochemical modelling of anaerobic vs. aerobic methane oxidation in a meromictic crater lake (Lake Pavin, France). Appl. Geochem. 26, 1919–1932.
Loux, N.T., 1998. An assessment of mercury-species-dependent binding with natural organic carbon. Chem. Speciat. Bioavailab. 10, 127–136.
Lu, X., Liu, Y., Johs, A., Zhao, L., Wang, T., Yang, Z., Lin, H., Elias, D.A., Pierce, E.M., Liang, L., 2016. Anaerobic mercury methylation and demethylation by Geobacter bemidjiensis Bem. Environ. Sci. Technol. 50, 4366–4373.
Malcolm, R., 1985. Geochemistry of stream fulvic and humic substances. Humic substances in soil, sediment, and water: geochemistry, isolation and characterization 181–209.
Martin, J.-M., 1985. Pavin Crater Lake. Chemical Processes in Lakes, vol. 1985. John Wiley and Sons, New York New York, pp. 169–188, 11 fig, 2 tab, 50 ref.
Mason, R., Lawson, N., Lawrence, A., Leaner, J., Lee, J., Sheu, G.-R., 1999. Mercury in the chesapeake bay. Mar. Chem. 65, 77–96.
Mason, R., Morel, F.a., Hemond, H., 1995. The role of microorganisms in elemental mercury formation in natural waters. Water Air Soil Pollut. 80, 775–787.

Mason, R.P., Choi, A.L., Fitzgerald, W.F., Hammerschmidt, C.R., Lamborg, C.H., Soerensen, A.L., Sunderland, E.M., 2012. Mercury biogeochemical cycling in the ocean and policy implications. Environ. Res. 119, 101–117.
Mercone, D., Thomson, J., Croudace, I., Troelstra, S., 1999. A coupled natural immobilisation mechanism for mercury and selenium in deep-sea sediments. Geochem. Cosmochim. Acta 63, 1481–1488.
Merritt, K.A., Amirbahman, A., 2007. Mercury dynamics in sulfide-rich sediments: geochemical influence on contaminant mobilization within the Penobscot River estuary, Maine, USA. Geochem. Cosmochim. Acta 71, 929–941.
Michard, G., Viollier, E., Jézéquel, D., Sarazin, G., 1994. Geochemical study of a crater lake: Pavin Lake, France—identification, location and quantification of the chemical reactions in the lake. Chem. Geol. 115, 103–115.
Miot, J., Jézéquel, D., Benzerara, K., Cordier, L., Rivas-Lamelo, S., Skouri-Panet, F., Férard, C., Poinsot, M., Duprat, E., 2016. Mineralogical diversity in Lake Pavin: connections with water column chemistry and biomineralization processes. Minerals 6, 24.
Muresan, B., Cossa, D., Coquery, M., Richard, S., 2008. Mercury sources and transformations in a man-perturbed tidal estuary: the Sinnamary Estuary, French Guiana. Geochem. Cosmochim. Acta 72, 5416–5430.
Muresan, B., Metzger, É., Jézéquel, D., Cossa, D., 2018. A multiscale study of mercury transformations and dynamics at the chemocline of the Petit-Saut tropical reservoir (French Guiana). Sci. Total Environ. 630, 1401–1412.
Oremland, R.S., Culbertson, C.W., Winfrey, M.R., 1991. Methylmercury decomposition in sediments and bacterial cultures: involvement of methanogens and sulfate reducers in oxidative demethylation. Appl. Environ. Microbiol. 57, 130–137.
Paranjape, A.R., Hall, B.D., 2017. Recent advances in the study of mercury methylation in aquatic systems. Facets 2, 85–119.
Parkhurst, D.L., Appelo, C., 2013. Description of input and examples for PHREEQC version 3—a computer program for speciation, batch-reaction, one-dimensional transport, and inverse geochemical calculations. US geological survey techniques and methods 6, 497.
Parks, J.M., Johs, A., Podar, M., Bridou, R., Hurt, R.A., Smith, S.D., Tomanicek, S.J., Qian, Y., Brown, S.D., Brandt, C.C., 2013. The genetic basis for bacterial mercury methylation. Science 339, 1332–1335.
Pempkowiak, J., Cossa, D., Sikora, A., Sanjuan, J., 1998. Mercury in water and sediments of the southern Baltic Sea. Sci. Total Environ. 213, 185–192.
Peretyazhko, T., Charlet, L., Grimaldi, M., 2006a. Production of gaseous mercury in hydromorphic soils in the presence of ferrous iron: a laboratory study. Eur. J. Soil Sci. 57, 190–199.
Peretyazhko, T., Charlet, L., Muresan, B., Kazimirov, V., Cossa, D., 2006b. Formation of dissolved gaseous mercury in a tropical lake (Petit-Saut reservoir, French Guiana). Sci. Total Environ. 364, 260–271.
Porcella, D.B., 1994. Mercury in the Environment: Biogeochemistry, Mercury Pollution Intergration and Synthesis, pp. 3–19.
Poulton, S.W., Canfield, D.E., 2011. Ferruginous conditions: a dominant feature of the ocean through Earth's history. Elements 7, 107–112.
Prahl, F., Small, L., Eversmeyer, B., 1997. Biogeochemical characterization of suspended particulate matter in the Columbia River estuary. Mar. Ecol. Prog. Ser. 160, 173–184.
Raimbault, P., Diaz, F., Pouvesle, W., Boudjellal, B., 1999. Simultaneous determination of particulate organic carbon, nitrogen and phosphorus collected on filters, using a semi-automatic wet-oxidation method. Mar. Ecol. Prog. Ser. 180, 289–295.
Regnell, O., Ewald, G., Lord, E., 1997. Factors controlling temporal variation in methyl mercury levels in sediment and water in a seasonally stratified lake. Limnol. Oceanogr. 42, 1784–1795.
Regnell, O., Tunlid, A., 1991. Laboratory study of chemical speciation of mercury in lake sediment and water under aerobic and anaerobic conditions. Appl. Environ. Microbiol. 57, 789–795.
Regnell, O., Watras, C.J., 2018. Microbial mercury methylation in aquatic environments: a critical review of published field and laboratory studies. Environ. Sci. Technol. 53, 4–19.
Riccardi, D., Guo, H.-B., Parks, J.M., Gu, B., Summers, A.O., Miller, S.M., Liang, L., Smith, J.C., 2013. Why mercury prefers soft ligands. J. Phys. Chem. Lett. 4, 2317–2322.
Rigaud, S., Radakovitch, O., Couture, R.-M., Deflandre, B., Cossa, D., Garnier, C., Garnier, J.-M., 2013. Mobility and fluxes of trace elements and nutrients at the sediment–water interface of a lagoon under contrasting water column oxygenation conditions. Appl. Geochem. 31, 35–51.
Rolfhus, K.R., Fitzgerald, W.F., 2004. Mechanisms and temporal variability of dissolved gaseous mercury production in coastal seawater. Mar. Chem. 90, 125–136.
Rosati, G., Heimbürger, L.-E., Melaku Canu, D., Lagane, C., Laffont, L., Rijkenberg, M.J., Gerringa, L.J., Solidoro, C., Gencarelli, C.N., Hedgecock, I.M., 2018. Mercury in the Black Sea: new insights from measurements and numerical modeling. Global Biogeochem. Cycles 32, 529–550.
Saiz-Lopez, A., Sitkiewicz, S.P., Roca-Sanjuán, D., Oliva-Enrich, J.M., Dávalos, J.Z., Notario, R., Jiskra, M., Xu, Y., Wang, F., Thackray, C.P., 2018. Photoreduction of gaseous oxidized mercury changes global atmospheric mercury speciation, transport and deposition. Nat. Commun. 9, 1–9.
Schaefer, J.K., Morel, F.M.M., 2009. High methylation rates of mercury bound to cysteine by Geobacter sulfurreducens. Nat. Geosci. 2, 123–126.
Skyllberg, U., 2008. Competition among thiols and inorganic sulfides and polysulfides for Hg and MeHg in wetland soils and sediments under suboxic conditions: illumination of controversies and implications for MeHg net production. J. Geophys. Res.: Biogeosciences 113, 2005-2012.
Skyllberg, U., Qian, J., Frech, W., Xia, K., Bleam, W.F., 2003. Distribution of mercury, methyl mercury and organic sulphur species in soil, soil solution and stream of a boreal forest catchment. Biogeochemistry 64, 53–76.
Slowey, A.J., Brown, J.G.E., 2007. Transformations of mercury, iron, and sulfur during the reductive dissolution of iron oxyhydroxide by sulfide. Geochem. Cosmochim. Acta 71, 877–894.
Smith, R.M., Martell, A.E., 1976. Critical Stability Constants: Inorganic Complexes. Springer.
Soerensen, A.L., Schartup, A., Skrobonja, A., Bouchet, S., Amouroux, D., Liem-Nguyen, V., Björn, E., 2018. Deciphering the role of water column redoxclines on methylmercury cycling using speciation modeling and observations from the Baltic Sea. Global Biogeochem. Cycles 32, 1498–1513.
Thouret, J.-C., Boivin, P., Labazuy, P., Leclerc, A., 2016. Geology, Geomorphology and Slope Instability of the Maar Lake Pavin (Auvergne, French Massif Central), Lake Pavin. Springer, pp. 155–174.
Tipping, E., 1994. WHAMC—a chemical equilibrium model and computer code for waters, sediments, and soils incorporating a discrete site/electrostatic model of ion-binding by humic substances. Comput. Geosci. 20, 973–1023.
Tisserand, D., Guédron, S., Razimbaud, S., Findling, N., Charlet, L., 2021. Acid Volatile Sulfides and Simultaneously Extracted Metals: A New Miniaturized 'purge and Trap' System for Laboratory and Field Measurements. Talanta, 122490.
Ullrich, S.M., Tanton, T.W., Abdrashitova, S.A., 2001. Mercury in the aquatic environment: a review of factors affecting methylation. Crit. Rev. Environ. Sci. Technol. 31, 241–293.
USEPA, USEPA, 1998. In: Method 1630: Methyl Mercury in Water by Distillation, Aqueous Ethylation,Purge and Trap, and Cold Vapor Atomic FluorescenceSpectrometry. U.S. Environmental Protection Agency USEPA, Washington.
USEPA, 2002. In: Method 1631, Revision E: Mercury in Water by Oxidation, Purge andTrap, and Cold Vapor Atomic FluorescenceSpectrometry. USEPA, Washington.
Viollier, E., Inglett, P.W., Hunter, K., Roychoudhury, A.N., Van Cappellen, P., 2000. The ferrozine method revisited: Fe (II)/Fe (III) determination in natural waters. Appl. Geochem. 15, 785–790.
Viollier, E., Michard, G., Jézéquel, D., Pèpe, M., Sarazin, G., 1997. Geochemical study of a crater lake: lake Pavin, Puy de Dôme, France. Constraints afforded by the particulate matter distribution in the element cycling within the lake. Chem. Geol. 142, 225–241.
Wang, Y., Liu, J., Liem-Nguyen, V., Tian, S., Zhang, S., Wang, D., Jiang, T., 2022. Binding strength of mercury (II) to different dissolved organic matter: the roles of DOM properties and sources. Sci. Total Environ. 807, 150979.
Watras, C., Bloom, N., 1994. The vertical distribution of mercury species in Wiskonsin Lakes: accumulation in plankton layers. In: Watras, C., Huckabee, J. (Eds.), Mercury Pollution: Integration and Synthesis. Lewis pub., pp. 137–185
Xia, K., Skyllberg, U., Bleam, W., Bloom, P., Nater, E., Helmke, P., 1999. X-ray absorption spectroscopic evidence for the complexation of Hg (II) by reduced sulfur in soil humic substances. Environ. Sci. Technol. 33, 257–261.
Yang, S., Johnson, W.P., Black, F.J., Rowland, R., Rumsey, C., Piskadlo, A., 2020. Response of density stratification, aquatic chemistry, and methylmercury to engineered and hydrologic forcings in an endorheic lake (Great Salt Lake, USA). Limnol. Oceanogr. 65, 915–926.
Zaferani, S., Pérez-Rodríguez, M., Biester, H., 2018. Diatom ooze—a large marine mercury sink. Science 361, 797–800.
Zheng, W., Liang, L., Gu, B., 2011. Mercury reduction and oxidation by reduced natural organic matter in anoxic environments. Environ. Sci. Technol. 46, 292–299.